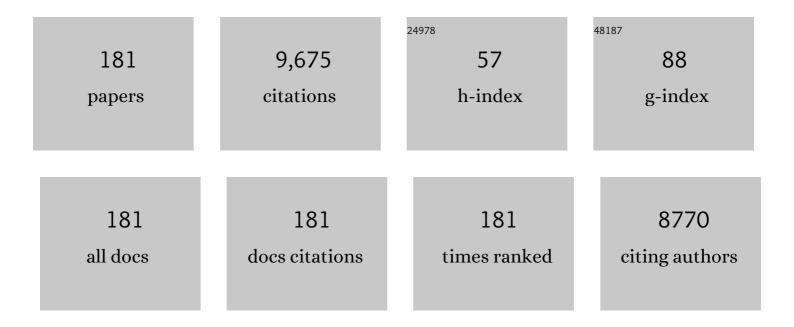
List of Publications by Year in descending order

Source: https://exaly.com/author-pdf/4151140/publications.pdf Version: 2024-02-01



ΥλΝ-Ηυι ΔΟ

#	Article	IF	CITATIONS
1	Kinetics and thermodynamics of adsorption of methylene blue by a magnetic graphene-carbon nanotube composite. Applied Surface Science, 2014, 290, 116-124.	3.1	292
2	Iodideâ€Induced Fragmentation of Polymerized Hydrophilic Carbon Nitride for Highâ€Performance Quasiâ€Homogeneous Photocatalytic H ₂ O ₂ Production. Angewandte Chemie - International Edition, 2021, 60, 25546-25550.	7.2	251
3	Synthesis of novel 2D-2D p-n heterojunction BiOBr/La 2 Ti 2 O 7 composite photocatalyst with enhanced photocatalytic performance under both UV and visible light irradiation. Applied Catalysis B: Environmental, 2016, 194, 157-168.	10.8	245
4	Facile synthesis of dual Z-scheme g-C3N4/Ag3PO4/AgI composite photocatalysts with enhanced performance for the degradation of a typical neonicotinoid pesticide. Applied Catalysis B: Environmental, 2020, 268, 118395.	10.8	225
5	Mediator-free direct dual-Z-scheme Bi2S3/BiVO4/MgIn2S4 composite photocatalysts with enhanced visible-light-driven performance towards carbamazepine degradation. Applied Catalysis B: Environmental, 2019, 254, 479-490.	10.8	217
6	Significantly enhanced visible light photocatalytic efficiency of phosphorus doped TiO2 with surface oxygen vacancies for ciprofloxacin degradation: Synergistic effect and intermediates analysis. Journal of Hazardous Materials, 2018, 351, 196-205.	6.5	204
7	Robust photocatalytic hydrogen evolution over amorphous ruthenium phosphide quantum dots modified g-C3N4 nanosheet. Applied Catalysis B: Environmental, 2018, 239, 578-585.	10.8	193
8	Visible light activated photocatalytic degradation of tetracycline by a magnetically separable composite photocatalyst: Graphene oxide/magnetite/cerium-doped titania. Journal of Colloid and Interface Science, 2016, 467, 129-139.	5.0	186
9	Rationally constructing of a novel dual Z-scheme composite photocatalyst with significantly enhanced performance for neonicotinoid degradation under visible light irradiation. Applied Catalysis B: Environmental, 2020, 270, 118918.	10.8	153
10	Low-temperature preparation of F-doped TiO2 film and its photocatalytic activity under solar light. Applied Surface Science, 2008, 254, 3033-3038.	3.1	151
11	All-solid-state Z-scheme WO3 nanorod/ZnIn2S4 composite photocatalysts for the effective degradation of nitenpyram under visible light irradiation. Journal of Hazardous Materials, 2020, 387, 121713.	6.5	147
12	Photocatalytic degradation of tetrabromobisphenol A by a magnetically separable graphene–TiO2 composite photocatalyst: Mechanism and intermediates analysis. Chemical Engineering Journal, 2015, 264, 113-124.	6.6	140
13	Synergetic effect of MoS2 and MXene on the enhanced H2 evolution performance of CdS under visible light irradiation. Applied Surface Science, 2019, 473, 11-19.	3.1	139
14	Construction of silver/graphitic-C3N4/bismuth tantalate Z-scheme photocatalyst with enhanced visible-light-driven performance for sulfamethoxazole degradation. Chemical Engineering Journal, 2019, 378, 122122.	6.6	138
15	Effect of CuO nanoparticles on the production and composition of extracellular polymeric substances and physicochemical stability of activated sludge flocs. Bioresource Technology, 2015, 176, 65-70.	4.8	134
16	Effect of oxygen vacancy on enhanced photocatalytic activity of reduced ZnO nanorod arrays. Applied Surface Science, 2015, 325, 112-116.	3.1	130
17	Mini Review on the Structure and Properties (Photocatalysis), and Preparation Techniques of Graphitic Carbon Nitride Nano-Based Particle, and Its Applications. Nanoscale Research Letters, 2018, 13, 388.	3.1	127
18	A one-pot method for the preparation of graphene–Bi2MoO6 hybrid photocatalysts that are responsive to visible-light and have excellent photocatalytic activity in the degradation of organic pollutants. Carbon, 2012, 50, 5256-5264.	5.4	125

#	Article	IF	CITATIONS
19	Combining Heterojunction Engineering with Surface Cocatalyst Modification To Synergistically Enhance the Photocatalytic Hydrogen Evolution Performance of Cadmium Sulfide Nanorods. ACS Sustainable Chemistry and Engineering, 2017, 5, 7670-7677.	3.2	123
20	Noble-metal-free nickel phosphide modified CdS/C ₃ N ₄ nanorods for dramatically enhanced photocatalytic hydrogen evolution under visible light irradiation. Dalton Transactions, 2017, 46, 13793-13801.	1.6	122
21	Efficient degradation of atrazine by BiOBr/UiO-66 composite photocatalyst under visible light irradiation: Environmental factors, mechanisms and degradation pathways. Chemosphere, 2018, 203, 497-505.	4.2	118
22	Boosting 2eâ^' oxygen reduction reaction in garland carbon nitride with carbon defects for high-efficient photocatalysis-self-Fenton degradation of 2,4-dichlorophenol. Applied Catalysis B: Environmental, 2022, 307, 121185.	10.8	118
23	Phosphate group grafted twinned BiPO4 with significantly enhanced photocatalytic activity: Synergistic effect of improved charge separation efficiency and redox ability. Applied Catalysis B: Environmental, 2018, 234, 90-99.	10.8	115
24	Synthesis of novel ternary heterogeneous anatase-TiO2 (B) biphase nanowires/Bi4O5I2 composite photocatalysts for the highly efficient degradation of acetaminophen under visible light irradiation. Journal of Hazardous Materials, 2020, 382, 121083.	6.5	115
25	In-situ construction of Z-scheme g-C3N4/WO3 composite with enhanced visible-light responsive performance for nitenpyram degradation. Chinese Chemical Letters, 2021, 32, 2179-2182.	4.8	108
26	Synthesis of Bi2O3–TiO2 composite film with high-photocatalytic activity under sunlight irradiation. Applied Surface Science, 2008, 255, 2365-2369.	3.1	103
27	Effects of CeO2 nanoparticles on production and physicochemical characteristics of extracellular polymeric substances in biofilms in sequencing batch biofilm reactor. Bioresource Technology, 2015, 194, 91-98.	4.8	103
28	Unraveling the Mechanism on Ultrahigh Efficiency Photocatalytic H ₂ O ₂ Generation for Dualâ€Heteroatom Incorporated Polymeric Carbon Nitride. Advanced Functional Materials, 2022, 32, .	7.8	100
29	Directing Charge Transfer in a Chemicalâ€Bonded BaTiO ₃ @ReS ₂ Schottky Heterojunction for Piezoelectric Enhanced Photocatalysis. Advanced Materials, 2022, 34, e2202508.	11.1	98
30	Inhibitory effects of ZnO nanoparticles on aerobic wastewater biofilms from oxygen concentration profiles determined by microelectrodes. Journal of Hazardous Materials, 2014, 276, 164-170.	6.5	95
31	Preparation of graphene–carbon nanotube–TiO2 composites with enhanced photocatalytic activity for the removal of dye and Cr (VI). Applied Catalysis A: General, 2014, 473, 83-89.	2.2	95
32	Photoelectrochemical property and photocatalytic activity of N-doped TiO2 nanotube arrays. Applied Surface Science, 2010, 256, 4397-4401.	3.1	94
33	Oxygen vacancies and phosphorus codoped black titania coated carbon nanotube composite photocatalyst with efficient photocatalytic performance for the degradation of acetaminophen under visible light irradiation. Chemical Engineering Journal, 2018, 352, 947-956.	6.6	92
34	Rationally constructing of a novel composite photocatalyst with multi charge transfer channels for highly efficient sulfamethoxazole elimination: Mechanism, degradation pathway and DFT calculation. Chemical Engineering Journal, 2021, 426, 131585.	6.6	89
35	Fabrication of novel p–n heterojunction BiOI/La ₂ Ti ₂ O ₇ composite photocatalysts for enhanced photocatalytic performance under visible light irradiation. Dalton Transactions, 2016, 45, 7986-7997.	1.6	88
36	Preparation, characterization, photocatalytic properties of titania hollow sphere doped with cerium. Journal of Hazardous Materials, 2010, 178, 517-521.	6.5	85

#	Article	IF	CITATIONS
37	Low-temperature preparation of Boron-doped titania by hydrothermal method and its photocatalytic activity. Journal of Alloys and Compounds, 2009, 484, 73-79.	2.8	83
38	Synergistic effect of molybdenum nitride nanoparticles and nitrogen-doped carbon on enhanced photocatalytic hydrogen evolution performance of CdS nanorods. Journal of Alloys and Compounds, 2020, 812, 151990.	2.8	80
39	Preparation of graphene oxide–Ag3PO4 composite photocatalyst with high visible light photocatalytic activity. Applied Surface Science, 2013, 271, 265-270.	3.1	76
40	Response of wastewater biofilm to CuO nanoparticle exposure in terms of extracellular polymeric substances and microbial community structure. Science of the Total Environment, 2017, 579, 588-597.	3.9	76
41	Prominent dual Z-scheme mechanism on phase junction WO3/CdS for enhanced visible-light-responsive photocatalytic performance on imidacloprid degradation. Separation and Purification Technology, 2022, 281, 119863.	3.9	76
42	Effects of water environmental factors on the photocatalytic degradation of sulfamethoxazole by Agl/UiO-66 composite under visible light irradiation. Journal of Alloys and Compounds, 2018, 748, 314-322.	2.8	73
43	Rational design of donor-acceptor conjugated polymers with high performance on peroxydisulfate activation for pollutants degradation. Applied Catalysis B: Environmental, 2022, 316, 121611.	10.8	73
44	A novel Ce, C-codoped TiO2 nanoparticles and its photocatalytic activity under visible light. Applied Surface Science, 2009, 256, 884-888.	3.1	72
45	Preparation of a ternary g-C3N4-CdS/Bi4O5I2 composite photocatalysts with two charge transfer pathways for efficient degradation of acetaminophen under visible light irradiation. Separation and Purification Technology, 2021, 259, 118177.	3.9	71
46	A simple route for the preparation of Eu, N-codoped TiO2 nanoparticles with enhanced visible light-induced photocatalytic activity. Journal of Colloid and Interface Science, 2008, 328, 447-451.	5.0	69
47	<i>In situ</i> surface engineering of ultrafine Ni ₂ P nanoparticles on cadmium sulfide for robust hydrogen evolution. Catalysis Science and Technology, 2018, 8, 5406-5415.	2.1	69
48	Dual-metal-driven Selective Pathway of Nitrogen Reduction in Orderly Atomic-hybridized Re ₂ MnS ₆ Ultrathin Nanosheets. Nano Letters, 2020, 20, 4960-4967.	4.5	69
49	Preparation, characterization and photocatalytic activity of the neodymium-doped TiO2 hollow spheres. Applied Surface Science, 2010, 257, 227-231.	3.1	68
50	Effects of CeO2 nanoparticles on biological nitrogen removal in a sequencing batch biofilm reactor and mechanism of toxicity. Bioresource Technology, 2015, 191, 73-78.	4.8	68
51	Effect of a typical antibiotic (tetracycline) on the aggregation of TiO2 nanoparticles in an aquatic environment. Journal of Hazardous Materials, 2018, 341, 187-197.	6.5	67
52	A simple method to prepare N-doped titania hollow spheres with high photocatalytic activity under visible light. Journal of Hazardous Materials, 2009, 167, 413-417.	6.5	66
53	In-situ synthesis of well dispersed CoP nanoparticles modified CdS nanorods composite with boosted performance for photocatalytic hydrogen evolution. International Journal of Hydrogen Energy, 2018, 43, 14934-14943.	3.8	64
54	Enhanced photoelectrocatalytic activity for dye degradation by graphene–titania composite film electrodes. Journal of Hazardous Materials, 2012, 223-224, 79-83.	6.5	63

#	Article	IF	CITATIONS
55	A simple method for the preparation of titania hollow sphere. Catalysis Communications, 2008, 9, 2574-2577.	1.6	61
56	Graphene and TiO2 co-modified flower-like Bi2O2CO3: A novel multi-heterojunction photocatalyst with enhanced photocatalytic activity. Applied Surface Science, 2015, 355, 411-418.	3.1	61
57	Preparation of CdS nanoparticle loaded flower-like Bi ₂ O ₂ CO ₃ heterojunction photocatalysts with enhanced visible light photocatalytic activity. Dalton Transactions, 2015, 44, 11321-11330.	1.6	60
58	In-depth insight into the mechanism on photocatalytic synergistic removal of antibiotics and Cr (â¥): The decisive effect of antibiotic molecular structure. Applied Catalysis B: Environmental, 2022, 313, 121443.	10.8	60
59	Maximizing the utilization of photo-generated electrons and holes of g-C3N4 photocatalyst for harmful algae inactivation. Chemical Engineering Journal, 2022, 431, 134105.	6.6	59
60	A simple method for large-scale preparation of ZnS nanoribbon film and its photocatalytic activity for dye degradation. Applied Surface Science, 2010, 256, 4125-4128.	3.1	56
61	Enhanced stability and dissolution of CuO nanoparticles by extracellular polymeric substances in aqueous environment. Journal of Nanoparticle Research, 2015, 17, 1.	0.8	53
62	Low-temperature preparation of anatase titania-coated magnetite. Journal of Physics and Chemistry of Solids, 2008, 69, 1980-1984.	1.9	49
63	Aggregation and removal of copper oxide (CuO) nanoparticles in wastewater environment and their effects on the microbial activities of wastewater biofilms. Bioresource Technology, 2016, 216, 537-544.	4.8	49
64	Construction of silver iodide/silver/bismuth tantalate Z-scheme photocatalyst for effective visible light degradation of organic pollutants. Journal of Colloid and Interface Science, 2018, 532, 190-200.	5.0	49
65	Piezo-enhanced photocatalytic performance of ZnO nanorod array for pollutants degradation in dynamic water: Insight into the effect of velocity and inner flow field. Nano Energy, 2022, 101, 107614.	8.2	49
66	A simple method for the preparation of Bi2WO6-reduced graphene oxide with enhanced photocatalytic activity under visible light irradiation. Materials Letters, 2013, 92, 126-128.	1.3	48
67	In-situ growth of Au and β-Bi2O3 nanoparticles on flower-like Bi2O2CO3: A multi-heterojunction photocatalyst with enhanced visible light responsive photocatalytic activity. Journal of Colloid and Interface Science, 2017, 495, 122-129.	5.0	48
68	Preparation of cerium and nitrogen co-doped titania hollow spheres with enhanced visible light photocatalytic performance. Powder Technology, 2011, 210, 203-207.	2.1	47
69	Synthesis of fluorine-doped titania-coated activated carbon under low temperature with high photocatalytic activity under visible light. Journal of Physics and Chemistry of Solids, 2008, 69, 2366-2370.	1.9	46
70	A simple route for the preparation of anatase titania-coated magnetic porous carbons with enhanced photocatalytic activity. Carbon, 2008, 46, 596-603.	5.4	46
71	A one-pot method to prepare N-doped titania hollow spheres with high photocatalytic activity under visible light. Applied Surface Science, 2010, 256, 2754-2758.	3.1	46
72	Effect of alginate on the aggregation kinetics of copper oxide nanoparticles (CuO NPs): bridging interaction and hetero-aggregation induced by Ca2+. Environmental Science and Pollution Research, 2016, 23, 11611-11619.	2.7	46

#	Article	IF	CITATIONS
73	Fabrication of noble-metal-free CdS nanorods-carbon layer-cobalt phosphide multiple heterojunctions for efficient and robust photocatalyst hydrogen evolution under visible light irradiation. Renewable Energy, 2019, 131, 180-186.	4.3	45
74	Bismuth oxychloride modified titanium phosphate nanoplates: A new p-n type heterostructured photocatalyst with high activity for the degradation of different kinds of organic pollutants. Journal of Colloid and Interface Science, 2016, 476, 71-78.	5.0	44
75	Preparation, characterization and photocatalytic activity of a novel composite photocatalyst: Ceria-coated activated carbon. Journal of Hazardous Materials, 2010, 184, 1-5.	6.5	43
76	Investigation on graphene and Pt co-modified CdS nanowires with enhanced photocatalytic hydrogen evolution activity under visible light irradiation. Dalton Transactions, 2015, 44, 16372-16382.	1.6	43
77	In-situ growth of Ag3VO4 nanoparticles onto BiOCl nanosheet to form a heterojunction photocatalyst with enhanced performance under visible light irradiation. Journal of Alloys and Compounds, 2016, 688, 1-7.	2.8	43
78	Effect of UV irradiation on the aggregation of TiO2 in an aquatic environment: Influence of humic acid and pH. Environmental Pollution, 2016, 212, 178-187.	3.7	43
79	Photoelectrocatalytic determination of chemical oxygen demand under visible light using Cu2O-loaded TiO2 nanotube arrays electrode. Sensors and Actuators B: Chemical, 2013, 181, 1-8.	4.0	42
80	Enhanced photocatalytic properties of the 3D flower-like Mg-Al layered double hydroxides decorated with Ag 2 CO 3 under visible light illumination. Materials Research Bulletin, 2016, 80, 23-29.	2.7	41
81	Adsorption of perfluorooctane sulfonate on soils: Effects of soil characteristics and phosphate competition. Chemosphere, 2017, 168, 1383-1388.	4.2	41
82	Preparation of Ag-doped mesoporous titania and its enhanced photocatalytic activity under UV light irradiation. Journal of Physics and Chemistry of Solids, 2008, 69, 2660-2664.	1.9	40
83	Magnetically separable composite photocatalyst with enhanced photocatalytic activity. Journal of Hazardous Materials, 2008, 160, 295-300.	6.5	40
84	Study on photocatalytic performance and degradation kinetics of X-3B with lanthanide-modified titanium dioxide under solar and UV illumination. Journal of Hazardous Materials, 2009, 164, 762-768.	6.5	40
85	A novel heterostructured plasmonic photocatalyst with high photocatalytic activity: Ag@AgCl nanoparticles modified titanium phosphate nanoplates. Journal of Alloys and Compounds, 2017, 698, 410-419.	2.8	40
86	Photocatalytic degradation of X-3B by titania-coated magnetic activated carbon under UV and visible irradiation. Journal of Alloys and Compounds, 2009, 471, 33-38.	2.8	39
87	Effects of interactions between humic acid and heavy metal ions on the aggregation of TiO2 nanoparticles in water environment. Environmental Pollution, 2019, 248, 834-844.	3.7	39
88	Understanding the mechanism of interfacial interaction enhancing photodegradation rate of pollutants at molecular level: Intermolecular π-π interactions favor electrons delivery. Journal of Hazardous Materials, 2022, 430, 128386.	6.5	39
89	Deposition of Ag@AgCl onto two dimensional square-like BiOCl nanoplates for high visible-light photocatalytic activity. Materials Letters, 2014, 131, 74-77.	1.3	38
90	Visible-light responsive C,N-codoped Titania hollow spheres for X-3B dye photodegradation. Microporous and Mesoporous Materials, 2009, 118, 382-386.	2.2	37

#	Article	IF	CITATIONS
91	Absorption and fluorescence characteristics of chromophoric dissolved organic matter in the Yangtze Estuary. Environmental Science and Pollution Research, 2014, 21, 3460-3473.	2.7	37
92	Effective inactivation of Microcystis aeruginosa by a novel Z-scheme composite photocatalyst under visible light irradiation. Science of the Total Environment, 2020, 746, 141149.	3.9	37
93	Construction of a composite photocatalyst with significantly enhanced photocatalytic performance through combination of homo-junction with hetero-junction. Catalysis Science and Technology, 2018, 8, 486-498.	2.1	36
94	A simple route to synthesize highly crystalline N-doped TiO2 particles under low temperature. Journal of Crystal Growth, 2008, 310, 4319-4324.	0.7	35
95	Synthesis of C,N,S-tridoped mesoporous titania with enhanced visible light-induced photocatalytic activity. Microporous and Mesoporous Materials, 2009, 122, 1-6.	2.2	35
96	Enhanced visible light activated hydrogen evolution activity over cadmium sulfide nanorods by the synergetic effect of a thin carbon layer and noble metal-free nickel phosphide cocatalyst. Journal of Colloid and Interface Science, 2018, 525, 107-114.	5.0	35
97	Modification strategies for enhancing the visible light responsive photocatalytic activity of the BiPO ₄ nano-based composite photocatalysts. Catalysis Science and Technology, 2019, 9, 546-566.	2.1	35
98	Photocatalytic activity on TiO2-coated side-glowing optical fiber reactor under solar light. Journal of Photochemistry and Photobiology A: Chemistry, 2008, 199, 165-169.	2.0	34
99	Adsorption behavior of lead on aquatic sediments contaminated with cerium dioxide nanoparticles. Environmental Pollution, 2016, 219, 416-424.	3.7	34
100	Preparation of porous titania thin film and its photocatalytic activity. Applied Surface Science, 2008, 255, 3137-3140.	3.1	31
101	Fabrication of p-type BiOCl/n-type La ₂ Ti ₂ O ₇ facet-coupling heterostructure with enhanced photocatalytic performance. RSC Advances, 2016, 6, 48599-48609.	1.7	31
102	Co-adsorption of perfluorooctane sulfonate and phosphate on boehmite: Influence of temperature, phosphate initial concentration and pH. Ecotoxicology and Environmental Safety, 2017, 137, 71-77.	2.9	31
103	Oxygen vacancies of the TiO ₂ nano-based composite photocatalysts in visible light responsive photocatalysis. RSC Advances, 2018, 8, 33551-33563.	1.7	31
104	2D ultrathin CoP modified Mn _x Cd _{1â^'x} S with controllable band structure and robust photocatalytic performance for hydrogen generation. Dalton Transactions, 2019, 48, 14783-14791.	1.6	31
105	0D/1D AgI/MoO3 Z-scheme heterojunction photocatalyst: Highly efficient visible-light-driven photocatalyst for sulfamethoxazole degradation. Chinese Chemical Letters, 2021, 32, 3226-3230.	4.8	31
106	Controlled synthesis in large-scale of CdS mesospheres and photocatalytic activity. Materials Letters, 2010, 64, 439-441.	1.3	29
107	Impacts of CuO nanoparticles on nitrogen removal in sequencing batch biofilm reactors after short-term and long-term exposure and the functions of natural organic matter. Environmental Science and Pollution Research, 2016, 23, 22116-22125.	2.7	29
108	Assessing the ecohydrological separation hypothesis and seasonal variations in water use by Ginkgo biloba L. in a subtropical riparian area. Journal of Hydrology, 2017, 553, 486-500.	2.3	29

#	Article	IF	CITATIONS
109	Interpretation of the disparity in harvesting efficiency of different types of Microcystis aeruginosa using polyethylenimine (PEI)-coated magnetic nanoparticles. Algal Research, 2018, 29, 257-265.	2.4	29
110	Highly efficient adsorption of uranium(<scp>vi</scp>) from aqueous solution by a novel adsorbent: titanium phosphate nanotubes. Environmental Science: Nano, 2018, 5, 2304-2314.	2.2	29
111	Preparation of Ag nanoparticles loaded TiO2 nanoplate arrays on activated carbon fibers with enhanced photocatalytic activity. Catalysis Communications, 2014, 53, 21-24.	1.6	28
112	A BiOBr/Co–Ni layered double hydroxide nanocomposite with excellent adsorption and photocatalytic properties. RSC Advances, 2015, 5, 54613-54621.	1.7	28
113	Photoproduction of dissolved organic carbon and inorganic nutrients from resuspended lake sediments. Environmental Science and Pollution Research, 2016, 23, 22126-22135.	2.7	28
114	Intimately coupled photocatalysis and biodegradation for effective simultaneous removal of sulfamethoxazole and COD from synthetic domestic wastewater. Journal of Hazardous Materials, 2022, 423, 127063.	6.5	28
115	Bi 2 MoO 6 nanosheets deposited TiO 2 nanobelts with spatially branched hierarchical heterostructure for enhanced photocatalytic activity under visible light irradiation. Colloids and Surfaces A: Physicochemical and Engineering Aspects, 2015, 487, 66-74.	2.3	26
116	Study on the effect of different acids on the structure and photocatalytic activity of mesoporous titania. Applied Surface Science, 2009, 256, 239-245.	3.1	25
117	Preparation, characterization of CdS-deposited graphene–carbon nanotubes hybrid photocatalysts with enhanced photocatalytic activity. Materials Letters, 2013, 108, 336-339.	1.3	25
118	Preparation of graphene oxide-loaded Ag3PO4@AgCl and its photocatalytic degradation of methylene blue and O2 evolution activity under visible light irradiation. International Journal of Hydrogen Energy, 2015, 40, 1016-1025.	3.8	25
119	ZnO nanorod arrays co-loaded with Au nanoparticles and reduced graphene oxide: Synthesis, characterization and photocatalytic application. Colloids and Surfaces A: Physicochemical and Engineering Aspects, 2016, 492, 71-78.	2.3	25
120	Regulating directional transfer of electrons on polymeric g-C3N5 for highly efficient photocatalytic H2O2 production. Journal of Colloid and Interface Science, 2022, 627, 739-748.	5.0	25
121	Long-term effects of CuO nanoparticles on the surface physicochemical properties of biofilms in a sequencing batch biofilm reactor. Applied Microbiology and Biotechnology, 2016, 100, 9629-9639.	1.7	24
122	Effects of pH and natural organic matter (NOM) on the adsorptive removal of CuO nanoparticles by periphyton. Environmental Science and Pollution Research, 2015, 22, 7696-7704.	2.7	23
123	Influence of silver nanoparticles on benthic oxygen consumption of microbial communities in freshwater sediments determined by microelectrodes. Environmental Pollution, 2017, 224, 771-778.	3.7	23
124	Photocatalytic properties of P25-doped TiO 2 composite film synthesized via sol–gel method on cement substrate. Journal of Environmental Sciences, 2018, 66, 71-80.	3.2	23
125	Synthesis of a magnetically separable composite photocatalyst with high photocatalytic activity under sunlight. Journal of Physics and Chemistry of Solids, 2009, 70, 1042-1047.	1.9	22
126	Photocatalytic activity of vanadium-doped titania–activated carbon composite film under visible light. Thin Solid Films, 2010, 518, 4170-4174.	0.8	22

#	Article	IF	CITATIONS
127	Hydrothermal synthesis of CeO2/NaNbO3 composites with enhanced photocatalytic performance. Chinese Journal of Catalysis, 2018, 39, 682-692.	6.9	22
128	Low temperature preparation of anatase TiO2-activated carbon composite film. Applied Surface Science, 2008, 254, 4001-4006.	3.1	21
129	Deposition of anatase titania onto carbon encapsulated magnetite nanoparticles. Nanotechnology, 2008, 19, 405604.	1.3	21
130	Preparation of a magnetic graphene oxide–Ag3PO4 composite photocatalyst with enhanced photocatalytic activity under visible light irradiation. Journal of the Taiwan Institute of Chemical Engineers, 2014, 45, 1080-1086.	2.7	21
131	Investigation on the application of titania nanorod arrays to the determination of chemical oxygen demand. Analytica Chimica Acta, 2013, 767, 141-147.	2.6	20
132	Influence of artificial ecological floating beds on river hydraulic characteristics. Journal of Hydrodynamics, 2014, 26, 474-481.	1.3	20
133	Long-term exposure to antibiotic mixtures favors microcystin synthesis and release in Microcystis aeruginosa with different morphologies. Chemosphere, 2019, 235, 344-353.	4.2	20
134	Investigation on Ce-doped TiO2-coated BDD composite electrode with high photoelectrocatalytic activity under visible light irradiation. Electrochemistry Communications, 2011, 13, 1423-1423.	2.3	19
135	Enhancing the hydrogen evolution performance of CdS by synergistic effect of Ni doping and SnO2 coupling: Improved efficiency of charge transfer and H2O disassociation. International Journal of Hydrogen Energy, 2021, 46, 6299-6309.	3.8	19
136	Preparation of B-doped titania hollow sphere and its photocatalytic activity under visible light. Materials Letters, 2009, 63, 2442-2444.	1.3	18
137	Preparation and enhanced photocatalytic performance of Sn ion modified titania hollow spheres. Materials Letters, 2011, 65, 3278-3280.	1.3	18
138	Influence of shear forces on the aggregation and sedimentation behavior of cerium dioxide (CeO2) nanoparticles under different hydrochemical conditions. Journal of Nanoparticle Research, 2016, 18, 1.	0.8	18
139	Titanium Phosphate Nanoplates Modified With AgBr@Ag Nanoparticles: A Novel Heterostructured Photocatalyst With Significantly Enhanced Visible Light Responsive Activity. Frontiers in Chemistry, 2018, 6, 489.	1.8	18
140	The surface engineering of ReS ₂ with cobalt for efficient performance in hydrogen evolution under both acid and alkaline conditions. Chemical Communications, 2020, 56, 8472-8475.	2.2	18
141	The performance of chitosan/montmorillonite nanocomposite during the flocculation and floc storage processes of Microcystis aeruginosa cells. Environmental Science and Pollution Research, 2015, 22, 11148-11161.	2.7	17
142	Ultrafast photocatalytic degradation of nitenpyram by 2D ultrathin Bi2WO6: mechanism, pathways and environmental factors. Rare Metals, 2022, 41, 2439-2452.	3.6	16
143	Preparation of graphene-modified TiO2 nanorod arrays with enhanced photocatalytic activity by a solvothermal method. Materials Letters, 2013, 101, 41-43.	1.3	15
144	Process Optimization for Microcystin-LR Adsorption onto Nano-sized Montmorillonite K10: Application of Response Surface Methodology. Water, Air, and Soil Pollution, 2014, 225, 1.	1.1	15

#	Article	IF	CITATIONS
145	Photocatalytic performance of Gd ion modified titania porous hollow spheres under visible light. Materials Letters, 2010, 64, 1003-1006.	1.3	14
146	In-situ growth of zinc tungstate nanorods on graphene for enhanced photocatalytic performance. Materials Research Bulletin, 2014, 57, 41-46.	2.7	14
147	The effects of extracellular polymeric substances on magnetic iron oxide nanoparticles stability and the removal of microcystin-LR in aqueous environments. Ecotoxicology and Environmental Safety, 2018, 148, 89-96.	2.9	14
148	Flexible g-C3N4-based photocatalytic membrane for efficient inactivation of harmful algae under visible light irradiation. Applied Surface Science, 2022, 601, 154270.	3.1	14
149	Photoelectrochemical application of hollow titania film. Electrochemistry Communications, 2008, 10, 1812-1814.	2.3	13
150	A novel p–n heterostructured photocatalyst for the efficient photocatalytic degradation of different kinds of organic compounds under irradiation of both ultraviolet and visible light. Dalton Transactions, 2016, 45, 13907-13916.	1.6	12
151	Synthesis of novel visible-light-driven p-n type heterojunction Cr 2 O 3 /La 2 Ti 2 O 7 photocatalysts with improved photocatalytic performance. Materials Letters, 2018, 220, 54-57.	1.3	12
152	Quantifying physical transport and local proliferation of phytoplankton downstream of an eutrophicated lake. Journal of Hydrology, 2020, 585, 124796.	2.3	11
153	Risk prediction of microcystins based on water quality surrogates: A case study in a eutrophicated urban river network. Environmental Pollution, 2021, 275, 116651.	3.7	11
154	Solvent-controlled preparation and photocatalytic properties of nanostructured TiO2 thin films with different morphologies. Materials Research Bulletin, 2014, 49, 223-228.	2.7	10
155	Graphene-wrapped bismuth oxychloride nanocomposites: Synthesis, characterization, and enhanced photodegradation of methylene blue. Materials Science in Semiconductor Processing, 2014, 27, 909-914.	1.9	10
156	Early diagenetic alterations of biogenic and reactive silica in the surface sediment of the Yangtze Estuary. Continental Shelf Research, 2015, 99, 1-11.	0.9	10
157	Preparation of heterostructured Ag@AgCl/La ₂ Ti ₂ O ₇ plasmonic photocatalysts with high visible light photocatalytic performance for the degradation of organic pollutants. RSC Advances, 2016, 6, 19223-19232.	1.7	10
158	Polymeric carbon nitride coated Nb-TiO2 nanorod arrays with enhanced photoelectrocatalytic activity under visible light irradiation. Inorganic Chemistry Communication, 2019, 101, 113-116.	1.8	10
159	Enhanced photoelectrocatalytic performance of TiO2 nanorod array under visible light irradiation: Synergistic effect of doping, heterojunction construction and cocatalyst deposition. Inorganic Chemistry Communication, 2019, 108, 107521.	1.8	9
160	Surface Properties and Environmental Transformations Controlling the Bioaccumulation and Toxicity of Cerium Oxide Nanoparticles: A Critical Review. Reviews of Environmental Contamination and Toxicology, 2020, 253, 155-206.	0.7	9
161	Total Phenolic, Flavonoid and Alkaloid Contents, Oxidative DNA Damage Protective and Antioxidant Properties of Methanol and Aqueous Extracts of Dissotis rotundifolia Whole Plant. Free Radicals and Antioxidants, 2018, 8, 82-88.	0.2	9
162	Probing the role of surface acid sites on the photocatalytic degradation of tetracycline hydrochloride over cerium doped CdS <i>via</i> experiments and theoretical calculations. Dalton Transactions, 2021, 50, 16620-16630.	1.6	9

#	Article	IF	CITATIONS
163	One-pot synthesis of AgBr/Ag2CO3 heterojunctions with enhanced visible-light photocatalytic activity. Materials Letters, 2016, 163, 258-261.	1.3	8
164	A simple method for preparation of superparamagnetic porous silica. Journal of Alloys and Compounds, 2010, 493, 410-414.	2.8	7
165	Response surface modeling and optimization of microcystin-LR removal from aqueous phase by polyacrylamide/sodium alginate–montmorillonite superabsorbent nanocomposite. Desalination and Water Treatment, 2015, 56, 1121-1139.	1.0	7
166	Graphene nanocrystals in CO2 photoreduction with H2O for fuel production. Nanoscale Advances, 2020, 2, 991-1006.	2.2	7
167	Iodideâ€Induced Fragmentation of Polymerized Hydrophilic Carbon Nitride for High Performance Quasiâ€Homogeneous Photocatalytic H2O2 Production. Angewandte Chemie, 0, , .	1.6	7
168	Surface Complex and Nonradical Pathways Contributing to High-Efficiency Degradation of Perfluorooctanoic Acid on Oxygen-Deficient In ₂ O ₃ Derived from an In-Based Metal Organic Framework. ACS ES&T Water, 2022, 2, 1344-1352.	2.3	7
169	In-situ growth of NiS co-catalyst on MnS/Mn0.3Cd0.7S heterojunction for boosting photocatalytic hydrogen evolution under visible light irradiation. Surfaces and Interfaces, 2021, 26, 101401.	1.5	6
170	Numerical simulation of microcystin distribution in Liangxi River, downstream of Taihu Lake. Water Environment Research, 2021, 93, 1934-1943.	1.3	6
171	Seasonal and spatial variations of acid-volatile sulphide and simultaneously extracted metals in the Yangtze River Estuary. Chemistry and Ecology, 2015, 31, 466-477.	0.6	5
172	Effect of light-active nanomaterials on the behavior of cadmium(II) in the presence of humic acid: the case of titanium dioxide. Desalination and Water Treatment, 2016, 57, 23975-23986.	1.0	4
173	Assessment of proliferative index in different grades of breast cancers using AgNOR (Agyrophilic) Tj ETQq1 1 0.7 7, 587-592.	84314 rgB 0.8	T /Overlock 3
174	Investigation of the rheological behavior of activated sludge in response to CeO2 nanoparticles and potential mechanism. Environmental Science and Pollution Research, 2018, 25, 29725-29733.	2.7	3
175	Synergistic effect of surface phase junction and surface defects on enhancing the photocatalytic performance of BiPO ₄ . Micro and Nano Letters, 2018, 13, 720-724.	0.6	3
176	Contributions of different fractions of extracellular polymeric substances from waste-activated sludge to Cu(II) biosorption. Desalination and Water Treatment, 2016, 57, 21405-21416.	1.0	2
177	Speciation of potentially mobile Si in Yangtze Estuary surface sediments: estimates using a modified sequential extraction technique. Environmental Science and Pollution Research, 2016, 23, 18928-18941.	2.7	2
178	DEVELOPMENT OF A MULTI-INDEX ECOSYSTEM HEALTH ASSESSMENT MODEL USING BACK-PROPAGATION NEURAL NETWORK APPROACH: A CASE STUDY OF THE YANGTZE ESTUARY, CHINA. Environmental Engineering and Management Journal, 2017, 16, 1551-1561.	0.2	1
179	Application of fuzzy mathematics in health assessment of estuarine ecosystem. , 2011, , .		0
180	Novel Visible Light Driven Magnetically Separable Graphene/BiOBr Composite Photocatalysts with Enhanced Photocatalytic Activity. Journal Wuhan University of Technology, Materials Science Edition, 2019, 34, 521-526.	0.4	0

#	Article	IF	CITATIONS
181	Comprehensive evaluation of kraft pulp properties from fast-growing woods. Tappi Journal, 2010, 9, 34-39.	0.2	0